Available online at www.sciencedirect.com
SCIENCE DIRECT®
International Journal of Multiphase Flow 31 (2005) 155–178
International Journal of Multiphase Flow
www.elsevier.com/locate/ijmulflow

A stochastic description of wall sources in a turbulent field. Part 3: Effect of gravitational settling on the concentration profiles

Yoichi Mito, Thomas J. Hanratty *

Department of Chemical and Biomolecular Engineering, University of Illinois, 205 Roger Adams Laboratory, Box C-3, 600 South Mathews Avenue, Urbana, IL 61801, USA

Received 20 April 2004; received in revised form 13 October 2004

Abstract

A stochastic method, which uses a modified Langevin equation to represent the fluid turbulence seen by the particles, is used to determine the fully-developed concentration profiles that exist for the turbulent flow of a dilute suspension of spheres in a horizontal channel. Particles with a wide range of inertial time constants and settling velocities are studied. The validity of using the Boussinesq approximation to represent turbulent mixing is explored.

Keywords: Disperse flow; Concentration profiles; Particle deposition; Turbulent mixing; Stochastic analysis; Langevin equation

1. Introduction

In horizontal flows of a suspension, gravity can greatly increase the rate of deposition over what would be observed in a vertical system (Mito and Hanratty, 2004a). This paper presents the results

* Corresponding author. Tel.: +1 217 333 1318; fax: +1 217 333 5052.
E-mail address: hanratty@scs.uiuc.edu (T.J. Hanratty).

0301-9322/$ - see front matter © 2004 Elsevier Ltd. All rights reserved.
doi:10.1016/j.ijmultiphaseflow.2004.10.002

of computer experiments which examine this phenomenon by determining concentration profiles. We show that distortions of the profiles are accompanied by increases in the deposition rate, but that large increases can also be experienced without changes in the symmetry of the concentration profile.

The work is motivated by our interest in gas–liquid flows, so the analysis is restricted to systems with large ratios of the densities of the particles to the densities of the fluid and for which particle interactions are not considered. An idealized representation of the disperse flow that exists in the core of an annular pattern is considered. Gas and spherical solid particles flow in a horizontal channel. Particles injected at the bottom and top walls eventually deposit. By adjusting the relative rates of admission of particles at the two walls, a fully-developed condition can be realized for which the net flux of particles in a direction perpendicular to the wall is zero at all locations in the channel. The two walls are considered to consist of arrays of point sources, so the theoretical problem is to calculate the behavior of a wall source.

The Lagrangian analysis of the trajectories of particles in a turbulent field has been advanced by carrying out studies in a direct numerical simulation of the carrier fluid. This type calculation is not feasible if one wants to study a large range of variables and large Reynolds numbers. The approach taken in this paper is to represent the fluid turbulence seen by the particles with a Langevin equation.

Concentration profiles of dispersed particles in horizontal pipes and channels have been studied with a Lagrangian approach by several investigators for cases in which deposition was not occurring. Sommerfeld and Zivkovic (1992) and Lun and Liu (1997) used $k-\varepsilon$ models to represent the mean fluid velocity field. Fluctuations seen by particles were sampled from an uncorrelated Gaussian distribution for randomly chosen eddy lifetimes (or interaction times), which results in an exponentially decaying autocorrelation function for the velocity fluctuations. (A discussion of eddy interaction models has been given by Graham (1996)). Oesterle and Petitjean (1993) used uncorrelated Gaussian random variables and experimental measurements to take account of the influence of fluid turbulence. Sommerfeld (2003) used a Langevin equation (Sommerfeld et al., 1993) to represent the fluid velocity fluctuations seen by particles. Zhang and Ahmadi (2000) carried out studies of deposition in a DNS of channel flow.

The chief contribution of the present paper is that it presents results over a very wide range of experimental conditions. The numerical approach is similar to what was used by Sommerfeld (2003) in that a Langevin equation is used. Despite the importance of the problem very few experimental investigations of concentration profiles in horizontal annular flow have been made. These include studies by Williams et al. (1996), Paras and Karaberas (1991) and some early works that are summarized by McCoy and Hanratty (1977).

A review of previous studies in this laboratory in which the Langevin equation is used to calculate particle dispersion is in order: Mito and Hanratty (2002) explored the use of a modified Langevin equation to describe the turbulent dispersion of fluid particles from point sources located at different locations in a channel. Good agreement with experiments in a DNS at $Re_\tau = 150$ and $Re_\tau = 300$ was realized. This method was also employed to describe wall sources of thermal markers. Fully-developed temperature profiles were calculated by picturing heated or cooled walls as consisting of arrays of sources or sinks. Again, excellent agreement was obtained with Eulerian calculations done in a DNS (Mito and Hanratty, 2003a). Iliopoulos et al. (2003) showed that the dispersion of solid particles from a point source in turbulent channel flow

can be described by using a modified Langevin equation to describe turbulent fluid velocity fluctuations seen by a particle.

These successes motivated a study which would provide a better understanding of particle dispersion and deposition of a dilute suspension of particles in the idealized model described above. In part 1 of this study (Mito and Hanratty, 2003b), the method was verified by comparing calculations for which the fluid turbulence is represented by the stochastic model and by a DNS. In Part 2 (Mito and Hanratty, 2004a) the stochastic method was used to study the mechanism of deposition over a much larger range of variables than had previously been explored, $\tau_p^+ = 3 - 40$ and $V_T^+ = 0 - 3.2$. Mito and Hanratty (2004b) also studied concentration profiles for the case of zero gravity.

This paper examines the effects of changes of τ_p^+ and V_τ^+ on the particle turbulence and on the characteristics of the concentration profile. The applicability of the Boussinesq approximation to represent turbulent mixing is also explored. Several previous works (Young and Leeming, 1997; Cerbelli et al., 2001; Mito and Hanratty, 2004b) used the Boussinesq approximation to describe turbulent mixing of solid particles in situations for which gravity is not an important consideration.

2. Computational method

2.1. Definition of system

Gas flows through infinitely wide horizontal parallel planes. The Reynolds number, $Re_\tau = 590$, is defined with the friction velocity, v^*, and the half-height of the channel, H. Cartesian coordinates x_1, x_2 and x_3 are assigned to the streamwise, wall-normal and spanwise directions. The channel walls are located at $x_2 = 0$ and at $x_2 = 2H$. Droplets are represented by solid spherical particles of diameter d_p. Gravity acts in the negative x_2 direction. Particles are treated as points and the concentration fields and other statistics are calculated based on the values of x_2 at their centers. Point sources are pictured to exist on both the bottom and top walls. Particles are injected from $x_2 = d_p/2$ with a velocity of (V_1^0, V_2^0, V_3^0) and a rate per unit area of R_{Ab} and from $x_2 = 2H - d_p/2$ with a velocity of $(V_1^0, -V_2^0, V_3^0)$ and a rate per unit area of R_{At}. These particles eventually deposit when they are a distance of $d_p/2$ from a wall. The rates of atomization at the bottom and top walls satisfy the conditions

$$R_{Ab} = R_{Db} \quad \text{and} \quad R_{At} = R_{Dt}, \tag{1}$$

where R_{Db} and R_{Dt} are the deposition fluxes at the bottom and top walls. Since net fluxes are zero at all x_2 the representation of the concentration field in terms of fundamental mechanisms responsible for particle transport and mixing is simplified.

Since dilute flows of particles which are much heavier than the gas are considered, lift forces, inter-particle collisions and the influences of the particles on the gas flow are ignored. The location and velocity of a particle are defined by the following equations:

$$\frac{dx_i}{dt} = V_i, \tag{2}$$

$$\frac{\mathrm{d}V_i}{\mathrm{d}t} = -\frac{3\rho_\mathrm{f} C_\mathrm{D}}{4 d_\mathrm{p} \rho_\mathrm{p}} |\boldsymbol{V} - \boldsymbol{U}|(V_i - U_i) + g_i, \tag{3}$$

where V_i is the velocity of the particle, U_i is the gas velocity seen by the particle, t is the time, ρ_p is the density of the particle, ρ_f is the density of the gas, and g_i is a component of the acceleration of gravity. In the system considered, $g_2 = -g$ and $g_1 = g_3 = 0$. The drag coefficient, C_D, is given by

$$C_\mathrm{D} = \frac{24}{Re_\mathrm{p}}(1 + 0.15 Re_\mathrm{p}^{0.687}), \tag{4}$$

where the particle Reynolds number, Re_p, is defined with d_p and the magnitude of the relative velocity $|\boldsymbol{U} - \boldsymbol{V}|$. Then the dimensionless inertial time constant of a particle, $\tau_\mathrm{p}^+ = \tau_\mathrm{p} v^{*2}/\nu$, is defined as

$$\tau_\mathrm{p}^+ = \frac{4 d_\mathrm{p}^+ (\rho_\mathrm{p}/\rho_\mathrm{f})}{3 C_\mathrm{D} |\boldsymbol{V}^+ - \boldsymbol{U}^+|}, \tag{5}$$

where ν is the kinematic viscosity of the gas and $d_\mathrm{p}^+ = d_\mathrm{p} v^*/\nu$. For a Stokes law resistance

$$\tau_\mathrm{p}^+ = \frac{d_\mathrm{p}^{+2} (\rho_\mathrm{p}/\rho_\mathrm{f})}{18}. \tag{6}$$

Since Stokes law is approximately valid for the conditions considered in this paper, Eq. (6) is used to define τ_p^+. The influence of gravity is represented either by the dimensionless free-fall velocity, $V_\mathrm{T}^+ = V_\mathrm{T}/v^*$, or by the dimensionless acceleration of gravity, $g^+ = g\nu/v^{*3}$. The free-fall velocity is calculated from Eq. (3) for the condition of $\mathrm{d}V_2/\mathrm{d}t = 0$ and $\boldsymbol{U} = 0$. The dimensionless acceleration of gravity is given as $g^+ = 1/2 Fr Re_\tau$, where Fr is the Froude number defined as $Fr = v^{*2}/2gH$. The dimensionless free-fall velocity is approximated as

$$V_\mathrm{T}^+ \cong \tau_\mathrm{p}^+ g^+, \tag{7}$$

which is exact for Stokes law resistance.

2.2. Stochastic method

A modified Langevin equation is used to calculate the change of the fluid velocity seen by a solid particle, $\mathrm{d}u_i$, over a time interval $\mathrm{d}t$:

$$\mathrm{d}\left(\frac{u_i}{\sigma_i}\right) = -\frac{u_i}{\sigma_i \tau_i}\mathrm{d}t + \overline{\mathrm{d}\mu_i} + \mathrm{d}\mu_i', \tag{8}$$

where u_i is the fluctuating component of the fluid velocity seen by the particle, σ_i is the Eulerian root-mean-square value of the fluid velocity fluctuation, τ_i is the Lagrangian time constant. The forcing function, $\mathrm{d}\mu_i$, is assumed to be jointly Gaussian (Mito and Hanratty, 2002). The mean drift, $\overline{\mathrm{d}\mu_i}$, and the covariances of the fluctuations are given as

$$\overline{\mathrm{d}\mu_i} = \frac{\partial\left(\frac{\overline{u_2 u_i}}{\sigma_i}\right)}{\partial x_2}\mathrm{d}t, \tag{9}$$

$$\overline{\mathrm{d}\mu_i' d\mu_j'} = \frac{\overline{u_i u_j}}{\sigma_i \sigma_j}\left(\frac{1}{\tau_i}+\frac{1}{\tau_j}\right)\mathrm{d}t, \tag{10}$$

where an overbar indicates an ensemble average. These equations and the numerical procedure for solving them are described, in detail, by Mito and Hanratty (2003b). The DNS database for turbulent channel flow at $Re_\tau = 590$, obtained by Moser et al. (1999), is used to provide the mean velocities of the fluid and the turbulent statistics that appear in Eqs. (8)–(10). The computational time step used in Eqs. (2), (3), (8) was $\Delta t^+ = \Delta t v^{*2}/v = 0.5$.

Eq. (8) requires the time constants characterizing the fluid turbulence seen by the particles. These can be different from the time constants characterizing the dispersion of fluid particles. The basic notion in using Eq. (8) was that the τ_i for fluid particles would need to be adjusted to recognize that the dispersing particles do not follow the fluid and that the ratio of the time constant used in Eq. (8) to the time constant characterizing the dispersion of fluid particles could be a function of the inertial time constants of the particles and their free-fall velocities. A preliminary study with finite V_T (Mito and Hanratty, 2003b) revealed that good results could be obtained by simply equating the τ_i in Eq. (8) to the time constant of the fluid particles. Values of these time constants can be found in the paper by Mito and Hanratty (2004a) for $Re_\tau = 590$. A more recent paper with $V_T = 0$ (Mito and Hanratty, 2004b) shows that τ_2 and τ_3 characterizing fluid turbulence seen by the particles are close to values obtained for the dispersion of fluid particles. Values of τ_1 are different but the calculations are relatively insensitive to the choice of τ_1.

Calculations were also carried out for $V_T^+ = 0$ and for $V_T^+ = 0.11$ in which the forcing function was skewed. [See Iliopoulos et al. (2003).] Very small differences in the calculated results were noted.

3. Theory

3.1. Deposition constants

A rate of deposition R_D is defined as the average of the rates of deposition at the bottom and top walls:

$$R_D = \frac{R_{Ab}}{2}\left(1+\frac{R_{At}}{R_{Ab}}\right). \tag{11}$$

A deposition constant $k_{DB}^+ = k_{DB}/v^*$ is defined with bulk mean concentration C_B and R_D,

$$\frac{k_{DB}}{v^*} = \left[\left(\frac{C_B v^*}{R_{Ab}}\right)\left(\frac{R_{Ab}}{R_D}\right)\right]^{-1}. \tag{12}$$

Thus, k_{DB}^+ is a function both of $C_B v^*/R_{Ab}$ and of R_{At}/R_{Ab}. The term R_D/R_{Ab} in Eq. (12) varies from 1 to 1/2 with changes of R_{At} from R_{Ab} to 0. The change in $C_B v^*/R_{Ab}$ is the dominant factor in determining changes in k_{DB}^+.

Values of k_{DB}^+ for $\tau_p^+ = 3, 5, 10, 20, 40$ (Mito and Hanratty, 2004a) are plotted against g^+ in Fig. 1a and against V_T^+ in Fig. 1b. A very large effect of V_T^+ (or g^+) on k_{DB}^+ is noted. Several flow regimes are observed: Concentration fields are almost symmetric, except for the near-wall region, for

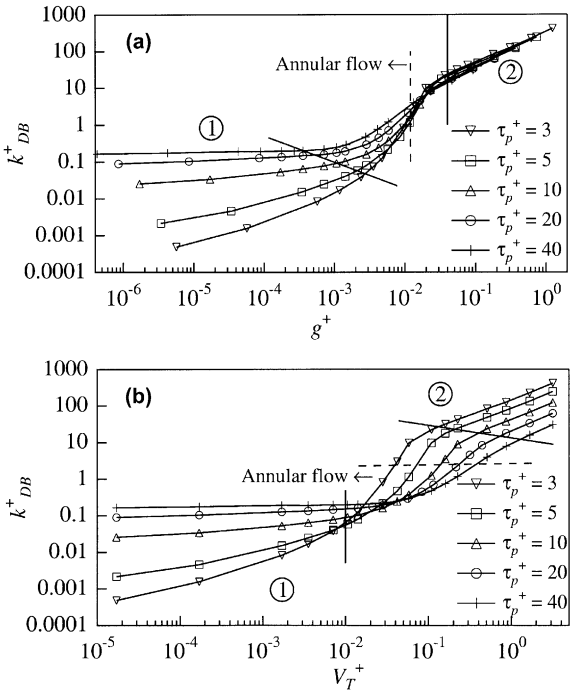

Fig. 1. Deposition constants: (a) effect of g^+ and (b) effect of V_{T}^+.

$V_{\mathrm{T}}^+ < 0.01$ (Region 1). A saltation pattern exists for $g^+ > 0.04$ (Region 2). The deposition constant can increase at surprisingly small values of V_{T}^+. The effect of gravity on k_{DB}^+ is quite strong in the region for which the concentration field is asymmetric ($V_{\mathrm{T}}^+ > 0.01$). A limit for which particles injected at the bottom wall can reach the top wall is observed at $g^+ = 0.012$. Thus, the annular flow regime is defined for $g^+ \leqslant 0.012$ (Region 3). It is noted that in the symmetric regime k_{DB}^+ increases very rapidly with increases of V_{T}^+ for $\tau_{\mathrm{p}}^+ = 3$ and 5 and is almost unchanged for $\tau_{\mathrm{p}}^+ = 20$ and 40. These features are related to changes in the concentration profiles described in the Section 4.

3.2. Diffusion model

A diffusion model can be derived from the ensemble-averaged mass balance equation by using a Boussinesq approximation for the turbulent mixing:

$$\frac{\partial}{\partial x_2}\left(\overline{C}\,\overline{V}_2 - \varepsilon\frac{\partial \overline{C}}{\partial x_2}\right) = 0, \tag{13}$$

where ε is the turbulent diffusivity. For a fully-developed concentration field, the total mass flux is zero at all x_2^+. Therefore, Eq. (13) can be simplified as

$$\overline{C}\,\overline{V}_2 - \varepsilon\frac{\partial \overline{C}}{\partial x_2} = 0, \tag{14}$$

or

$$\frac{\partial \ln \overline{C}}{\partial x_2} = \frac{\overline{V}_2}{\varepsilon}. \tag{15}$$

A mean convective velocity $\overline{V}_2$ is obtained from the ensemble-average of Eq. (3) as

$$\overline{V}_2 = -\overline{\tau_p \frac{dV_2}{dt}} - \bar{\tau}_p g = V_{tp} + V_g. \tag{16}$$

where the first term in the right-hand side of Eq. (16) represents the turbophoretic velocity, V_{tp}, and the second term represents the velocity induced by gravity, V_g, which is approximately equal to the terminal velocity, $-V_T$. If the dominant contributor to $\overline{V}_2$ is the settling velocity, V_T, and if $\varepsilon =$ constant (which could be plausible in the center region of the channel)

$$\overline{C} = C_0 \exp\left(-\frac{V_T}{\varepsilon} x_2\right), \tag{17}$$

where C_0 is a constant of integration. Deviations from Eq. (17) are expected in the near-wall regions because of the variation of ε with x_2 and the increasing contribution of V_{tp} to $\overline{V}_2$.

3.3. Turbophoretic velocity

Caporaloni et al. (1975) and Reeks (1983) have presented the notion that a drift velocity is created by a gradient in the particle velocity fluctuations

$$V_{tp} = -\bar{\tau}_p \frac{\partial \overline{v_2^2}}{\partial x_2}, \tag{18}$$

where $V_2 = \overline{V}_2 + v_2$ is the velocity in the x_2 direction. James B. Young and Hanratty (1991) presented laboratory measurements of $\overline{dV_2/dt}$ and showed that Eq. (18) can be obtained from the mean acceleration if an incompressibility assumption is made, whereby the influence of changes in particle concentration is ignored. John Young and Leeming (1997) presented a thorough investigation of this idea and derived an equation, which includes compressibility effects:

$$\overline{\frac{dV_2}{dt}} = \overline{V}_2 \frac{\partial \overline{V}_2}{\partial x_2} + \frac{\partial \overline{v_2^2}}{\partial x_2} + \overline{v_2 V_i \frac{\partial (\ln C)}{\partial x_i}}. \tag{19}$$

Cerbelli et al. (2001) used the following approximation:

$$\overline{v_2 V_i \frac{\partial (\ln C)}{\partial x_i}} \cong \overline{v_2^2} \frac{\partial (\ln \overline{C})}{\partial x_2}. \tag{20}$$

Mito and Hanratty (2004b) showed for the case of $g = 0$ that compressibility effects need to be taken into consideration in evaluating the turbophoretic velocity and that Eq. (20) does a satisfactory job.

3.4. Secondary maximum

Since particles are injected with a uniform velocity from the wall, a local maximum associated with a slowdown of the injected particles can be observed near the wall. Velocities of a particle

injected into a quiescent ambience, V_2^+, can be approximated by using Eq. (3) and the assumption of $\boldsymbol{U} = 0$. A concentration field in which particles enter the field at the bottom wall is calculated by assuming that the mass flux of the injected particles in the wall-normal direction is kept constant at R_{Ab} from the injection height to the top of the trajectories, so that

$$\frac{Cv^*}{R_{\mathrm{Ab}}} = \frac{1}{V_2^+}. \tag{21}$$

Fig. 2a presents the calculated concentration profiles of particles with $\tau_{\mathrm{p}}^+ = 3$ for $V_{\mathrm{T}}^+ = 0$, 0.014, 0.058, 0.11 when particles are being injected at $x_2^+ = d_{\mathrm{p}}^+/2 = 0.184$ with an initial velocity of 1 v^* in the wall-normal direction. The concentrations become infinite at the peaks of the trajectories, which are observed at $x_2^+ = 3.07$, 2.89, 2.58, 2.34. The concentrations increase very rapidly near the peaks. The distance from the wall to the peak decreases with increasing V_{T}^+. When the drag acting on a particle is Stokesian, that is, $\tau_{\mathrm{p}}^+ = \text{constant}$, the local maxima occur at

$$x_2^+ = \frac{d_{\mathrm{p}}^+}{2} + \tau_{\mathrm{p}}^+ \left[V_2^{0+} - V_{\mathrm{T}}^+ \ln\left(1 + \frac{V_2^{0+}}{V_{\mathrm{T}}^+}\right)\right]. \tag{22}$$

Thus, x_2^+ is a function of $d_{\mathrm{p}}^+, \tau_{\mathrm{p}}^+, V_{\mathrm{T}}^+$ and V_2^{0+}. Eq. (22) gives $x_2^+ = d_{\mathrm{p}}^+/2 + \tau_{\mathrm{p}}^+ V_2^{0+}$ when $V_{\mathrm{T}}^+ = 0$. The values of x_2^+ at the local maxima shown in Fig. 2a are seen to be slightly smaller than the values calculated from Eq. (22). This is because the fluid drag is non-Stokesian and the mean inertial time constants over the particle trajectories are smaller than the Stokesian inertial time constant. When

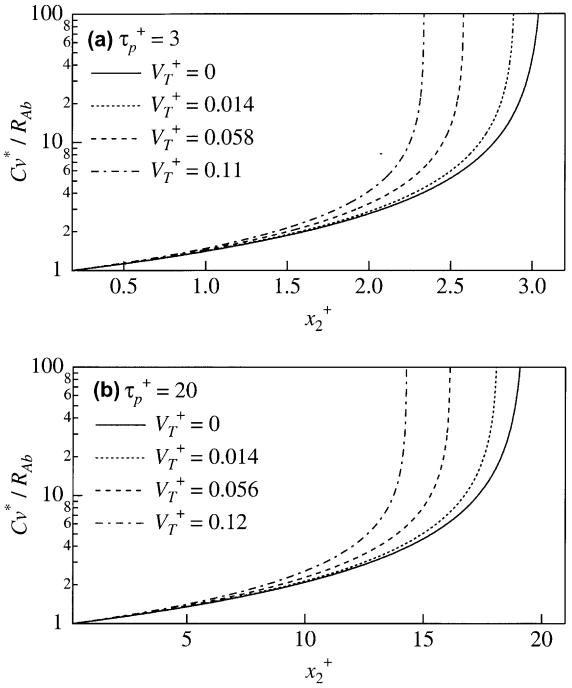

Fig. 2. Secondary maxima in concentration fields (a) for $\tau_{\mathrm{p}}^+ = 3$ and (b) for $\tau_{\mathrm{p}}^+ = 20$.

fluid turbulence exists, the distances from the wall to the local maxima decrease because of turbulent mixing.

Fig. 2b presents the increases of concentrations due to slowdowns of injected particles with $\tau_p^+ = 20$ for $V_T^+ = 0$, 0.014, 0.056, 0.12. Peaks are seen at $x_2^+ = 19.3$, 18.1, 16.1, 14.3. It is noted that, for this case, the local maxima exist in the buffer region, where the injected particles are subjected to strong turbulent mixing.

Fig. 3a presents velocities of the particles in the concentration fields for $\tau_p^+ = 3$. Fluid turbulence intensities in the wall-normal direction are also presented. It is noted that the fluid turbulence intensity is comparable to the particle velocity only near the local maxima. If the fluid drag acting on a particle is Stokesian,

$$V_2^+ = -\frac{x_2^+}{\tau_p^+} + V_2^{0+} - g^+ t^+, \tag{23}$$

where $t^+ (= tv^{*2}/v)$ is the dimensionless time for which the particle has been in the field. The curve for $V_T^+ = 0$ ($g^+ = 0$) is observed to have a slope of $-1/\tau_p^+$. This behavior is also observed for the curves for $V_T^+ \neq 0$ at small times (in the near-wall region). Fig. 3b presents velocities of the particles in the concentration fields shown in Fig. 2b. It is noted that the fluid turbulence is comparable to the particle velocity at $x_2^+ \approx 11$ for $\tau_p^+ = 20$, so particles should be strongly affected by turbulent mixing near this height.

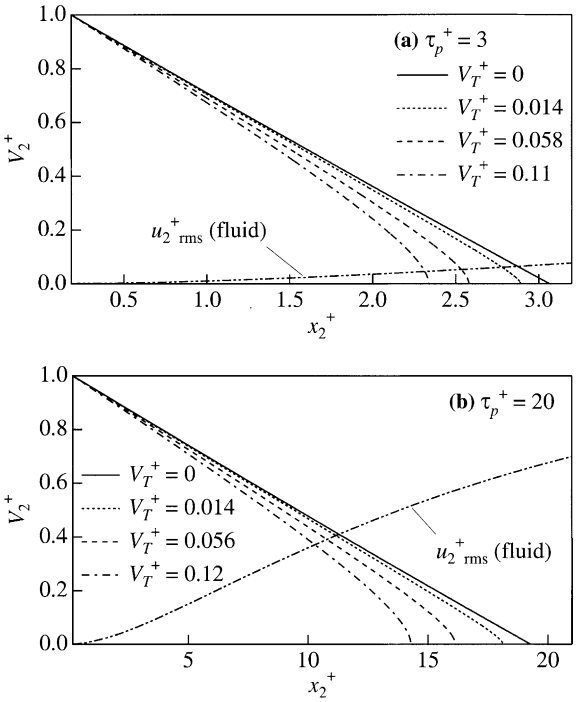

Fig. 3. Mean velocities of the particles generating secondary maxima (a) for $\tau_p^+ = 3$ and (b) for $\tau_p^+ = 20$.

4. Results

4.1. Scope of calculations

The computation of the behavior of a source involved the injection of N_b ($= 10^4$–10^7) particles from the bottom wall at time zero. Fully-developed concentration profiles were calculated from these results by methods outlined by Mito and Hanratty (2003b). The number of particles was increased until statistically steady results were obtained. When a strong asymmetry appears in the concentration field, the number of the injected particles needs to be increased in order to have enough samples in the upper region. The injection velocity was $\boldsymbol{V}^{0+} = (15, 1, 0)$. When particles deposited at the top wall, the same number was injected with $\boldsymbol{V}^{0+} = (15, -1, 0)$. The rate of atomization at the bottom wall is $N_b/A\Delta t$, where A is the area of the wall over which the particles are discharged and Δt is the time interval over which N_b particles are admitted from a wall source.

Calculations were done for a dimensionless particle diameter, $d_p^+ = 0.368$. Five inertial time constants, $\tau_p^+ = 3$, 5, 10, 20, 40, for which density ratios, ρ_p/ρ_f, are, respectively, 400, 665, 1325, 2650, 5300, are considered. The Froude number was varied so as to consider free-fall velocities in the range of $0 \leqslant V_T^+ \leqslant 3.2$. For example, the Froude numbers were varied from infinity to 6.9×10^{-4} for $\tau_p^+ = 3$ and from infinity to 9.2×10^{-4} for $\tau_p^+ = 40$, where the dimensionless accelerations of gravity, g^+, were varied from 0 to 1.2 for $\tau_p^+ = 3$ and from 0 to 0.93 for $\tau_p^+ = 40$.

The computations of the behavior of a wall source were performed until all of the particles injected at $t^+ = 0$ deposited. The integration time ranges from $t^+ = 1 \times 10^7$ to $t^+ = 2$ for $\tau_p^+ = 3$ and $0 \leqslant V_T^+ \leqslant 3.2$ and from $t^+ = 5 \times 10^4$ to $t^+ = 20$ for $\tau_p^+ = 40$ and $0 \leqslant V_T^+ \leqslant 3.2$.

4.2. Particle turbulence

Calculations by Mito and Hanratty (2004b) for $V_T^+ = 0$ show a decrease in $(\overline{v_2^2})^{1/2}$ with increasing τ_p^+. The influence of V_T^+ on $(\overline{v_2^2})^{1/2}$ is depicted in Figs. 4 and 5 for $\tau_p^+ = 3$ and for $\tau_p^+ = 20$. The contributions of recently injected particles are included in the evaluation of $(\overline{v_2^2})^{1/2}$. Values for the root-mean-square of the fluid velocity fluctuations, $(\overline{u_2^2})^{1/2}$, are also shown in Fig. 4. It is noted, both for $\tau_p^+ = 3$ and $\tau_p^+ = 20$, that $(\overline{v_2^2})^{1/2}$ is not affected by gravitational settling over most of the field.

An effect of V_T is noted for small x_2^+, as shown in Figs. 4b and 5b. This is observed in the region where direct contributions of the injected particles are important. As shown by Mito and Hanratty (2004b), the particle turbulence at $x_2^+ = d_p^+/2$ is given by

$$\overline{v_2^2} = -V_2^0 \overline{V}_d, \tag{24}$$

where $\overline{V}_d$ is the average velocity with which the particles strike the wall and V_2^0 is the component of the injection velocity in the x_2 direction. The observed increase in $(\overline{v_2^2})^{1/2}$ at the wall, with increasing V_T (or $\overline{V}_d$), is consistent with Eq. (24).

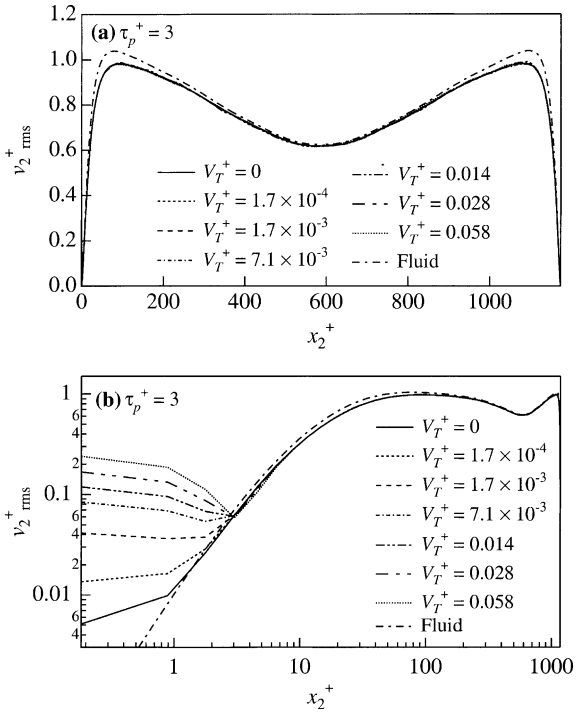

Fig. 4. Root-mean-square values of the wall-normal fluctuating component of particle velocity for $\tau_p^+ = 3$ in (a) arithmetic and (b) logarithmic coordinates.

4.3. Turbophoretic velocities

Turbophoretic velocities were obtained from calculations of $-\overline{\tau_p(dV_2/dt)}$. These are shown in Fig. 6 for $\tau_p^+ = 3$ and $\tau_p^+ = 20$. The minima reflect the variation of the particle turbulence with x_2 close to the wall in that they correspond approximately to the maximum in $\overline{v_2^2}$. However, the effect of V_T cannot be explained in this way since, as shown in Figs. 4 and 5, gravitational settling is not having a strong effect on $\overline{v_2^2}$. The individual terms on the right side of Eq. (19) that contribute to the mean acceleration, $\overline{dV_2/dt}$, were calculated (not shown). The first was found to be negligibly small compared to the other terms regardless of x_2^+, τ_p^+ or V_T^+. This was also observed for the cases of $V_T = 0$ by Mito and Hanratty (2004b). Therefore the behavior shown in Fig. 6 mainly reflects the changes in $\overline{v_2^2}$ and in the concentration field, indicated in the third term on the right side of Eq. (19).

4.4. Concentration profiles

Concentration profiles for $V_T^+ = 0$–0.11 and $\tau_p^+ = 3$ are plotted in Fig. 7a with semilogarithmic coordinates. The dotted lines represent Eq. (17) with $\varepsilon = 55\nu$ ($= 0.094 v^* H$). The values of C_0 are selected to fit the concentration curves in the center region of the channel. Eq. (17) is seen to give good approximations for the concentrations at $50 < x_2^+ < 2H^+ - 50$. This suggests that the

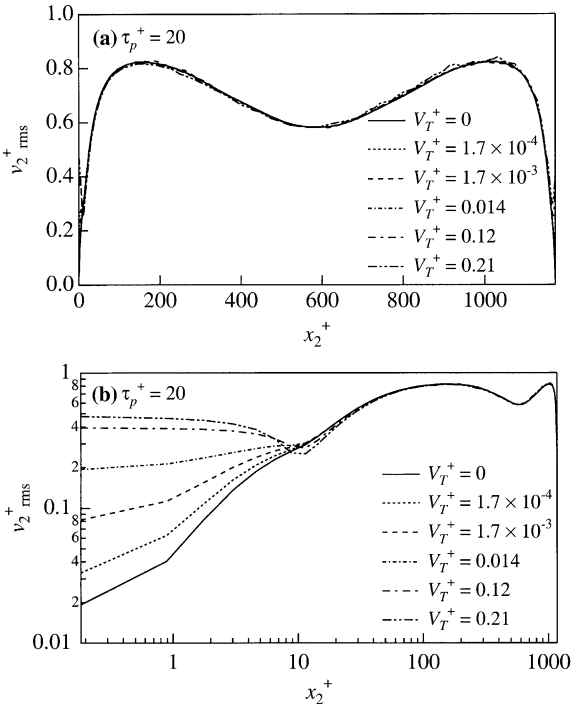

Fig. 5. Root-mean-square values of the wall-normal fluctuating component of particle velocity for $\tau_p^+ = 20$ in (a) arithmetic and (b) logarithmic coordinates.

concentration field in this region can be represented as a balance between diffusion and gravitational settling. Particles with $\tau_p^+ = 3$ injected at the bottom wall can strike the top wall only for $V_T^+ \leqslant 1.7 \times 10^{-4}$.

Large spatial changes in the concentration fields occur at $x_2^+ < 50$ and $x_2^+ > 2H^+ - 50$. Buildups of particles in these regions are caused mainly by large turbophoretic velocities, which are negative near the bottom wall and are positive near the top wall for the situations presented in Fig. 7. A more detailed examination of the concentration field close to the bottom wall is given in the log-log plot in Fig. 7b. Very thin boundary layers are observed for $V_T^+ \leqslant 1.7 \times 10^{-4}$ in the vicinity of the wall ($x_2^+ < 0.3$), where the terminal velocities are smaller than the turbulent fluid velocities at a distance of $d_p^+/2$ above the wall. The boundary layer disappears at $V_T^+ = 1.7 \times 10^{-3}$ because gravitational settling replaces turbulent impaction as the main mechanism for deposition (Mito and Hanratty, 2004a).

The concentration profiles for $\tau_p^+ = 3$ are approximately symmetric, except in the near-wall regions, for $V_T^+ < 0.01$ and the shapes are almost unchanged from what is observed for $V_T^+ = 0$ because of the very small effect of gravitational settling. It is noted that the concentration at a given x_2^+ decreases very rapidly with increases of V_T^+ for $V_T^+ < 0.01$. This decrease of the dimensionless bulk concentration (or increase in k_{DB}^+) with increases of V_T^+ for $1.7 \times 10^{-4} < V_T^+ < 0.01$ is attributed to the increase in the mean velocity of the depositing particles at the bottom wall, $\overline{V}_d^+$, due to the increase in the settling velocity. Thus, since $R_{Ab} \cong -\overline{V}_d \overline{C}_w$ in this region, the dimensionless

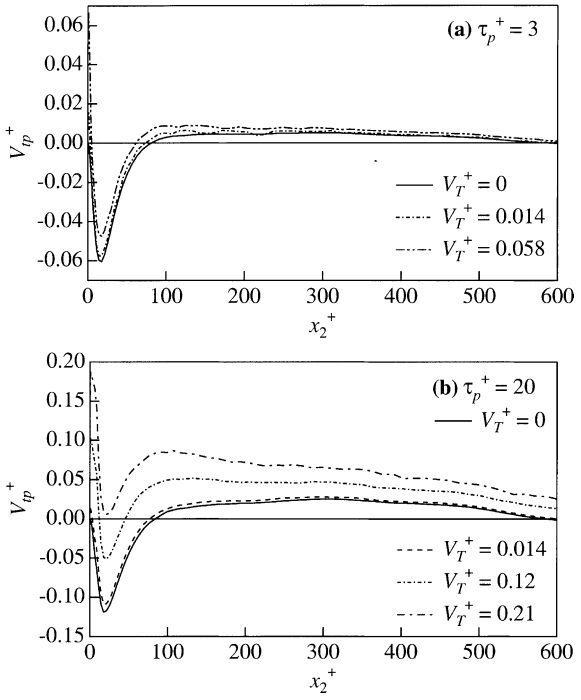

Fig. 6. Turbophoretic velocities (a) for $\tau_p^+ = 3$ and (b) for $\tau_p^+ = 20$.

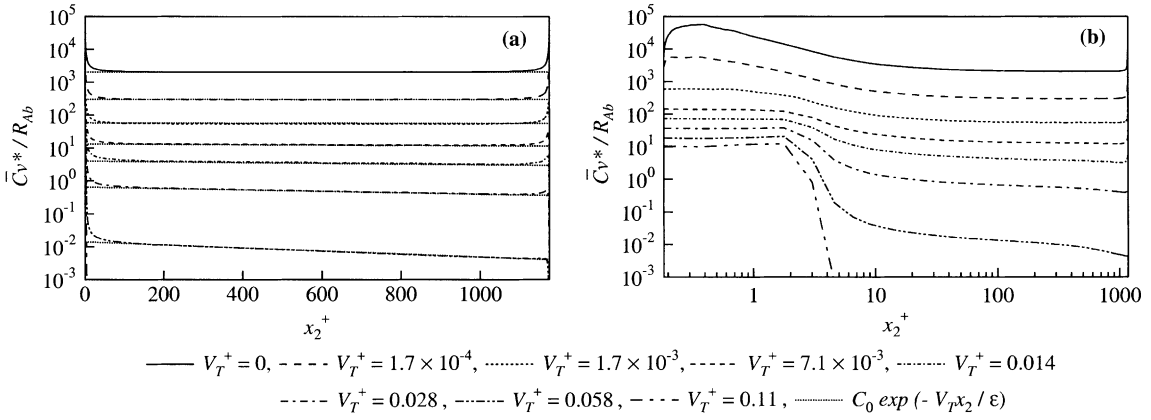

Fig. 7. Concentration profiles for $\tau_p^+ = 3$ plotted against (a) arithmetic and (b) logarithmic abscissae.

wall concentration $\overline{C}_w v^*/R_{Ab}$ decreases if $\overline{V}_d^+$ increases. (See Fig. 12.) For $V_T^+ \leqslant 1.7 \times 10^{-4}$ the deposition velocity does not change significantly with V_T^+ so $C_w v^*/R_{Ab}$ is roughly constant (see Fig. 12). The increase of $\overline{C}v^*/R_{Ab}$ at a fixed x_2^+ with decreases of V_T^+ for $V_T^+ \leqslant 1.7 \times 10^{-4}$ is associated with the increase in the concentration change in the boundary layer in the immediate vicinity of the wall.

Concentration profiles for $\tau_p^+ = 5, 10, 20, 40$ are presented in Figs. 8–11. Their features are similar to what is observed for $\tau_p^+ = 3$. Again, the dashed lines in Figs. 8–11a represent Eq. (17). The same value of ε is used in all of these comparisons. Deviations from Eq. (17) are observed at $x_2^+ < 100$, $x_2^+ < 150$, $x_2^+ < 200$, $x_2^+ < 300$ for $\tau_p^+ = 5$, 10, 20, 40, respectively. Particles injected from the bottom wall do not strike the top wall for $V_T^+ \geqslant 0.11$, 0.16, 0.31, 0.51 at $\tau_p^+ = 5$, 10, 20, 40. These results indicate that the limit of annular flow can be roughly defined as $g^+ \leqslant 0.012$ for this range τ_p^+. This criterion is observed to be much larger than what is found for $\tau_p^+ = 3$, because free-flight is contributing to deposition at the top wall for $\tau_p^+ \geqslant 5$, and not for $\tau_p^+ = 3$. The saltation regime starts at $V_T^+ = 0.23$, 0.51, 0.86, 1.7 for $\tau_p^+ = 5$, 10, 20, 40, that is, at $g^+ >$ ca. 0.04.

Changes in the magnitudes of the concentrations at a given x_2^+, associated with increases in V_T^+, decrease with increasing τ_p^+ for $V_T^+ < 0.01$. This is consistent with the small changes in the deposition constant with increasing V_T^+ shown in Fig. 1. It is noted that, except for the near-wall region, the concentration is almost unchanged with increases of V_T^+ for $V_T^+ < 0.01$ when $\tau_p^+ = 20$ and 40.

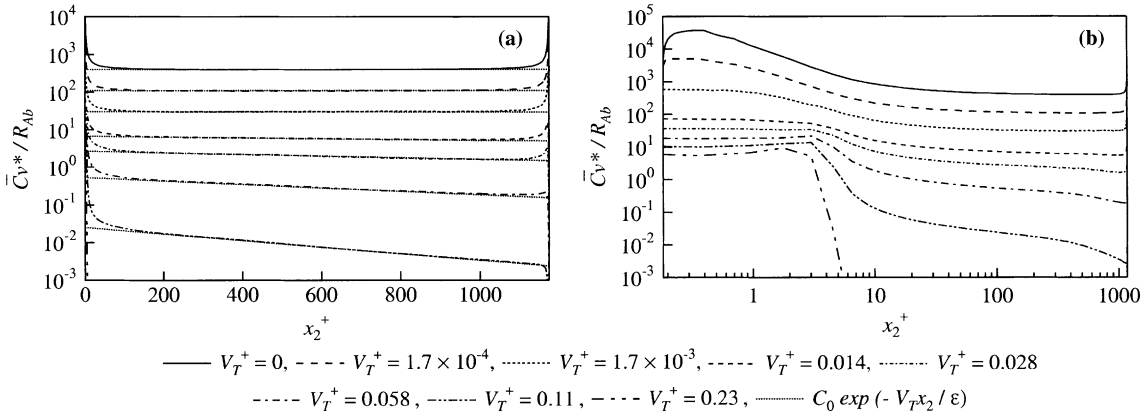

Fig. 8. Concentration profiles for $\tau_p^+ = 5$ plotted against (a) arithmetic and (b) logarithmic abscissae.

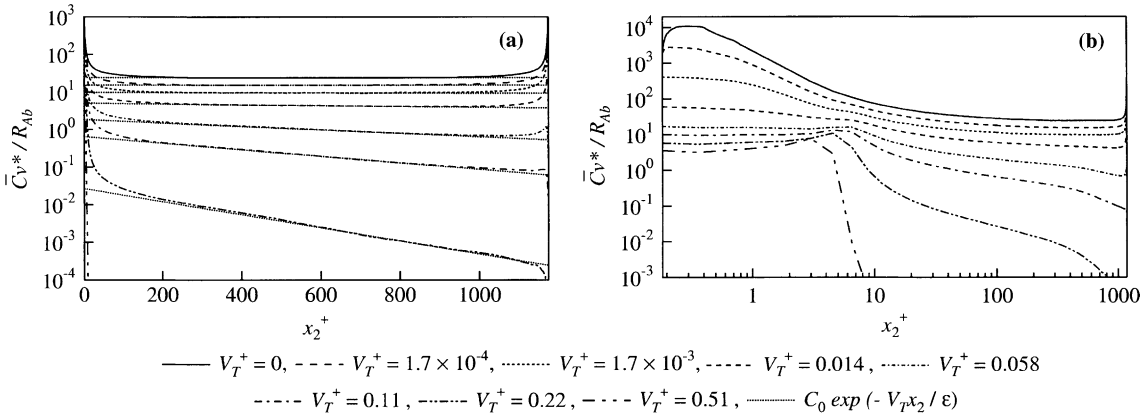

Fig. 9. Concentration profiles for $\tau_p^+ = 10$ plotted against (a) arithmetic and (b) logarithmic abscissae.

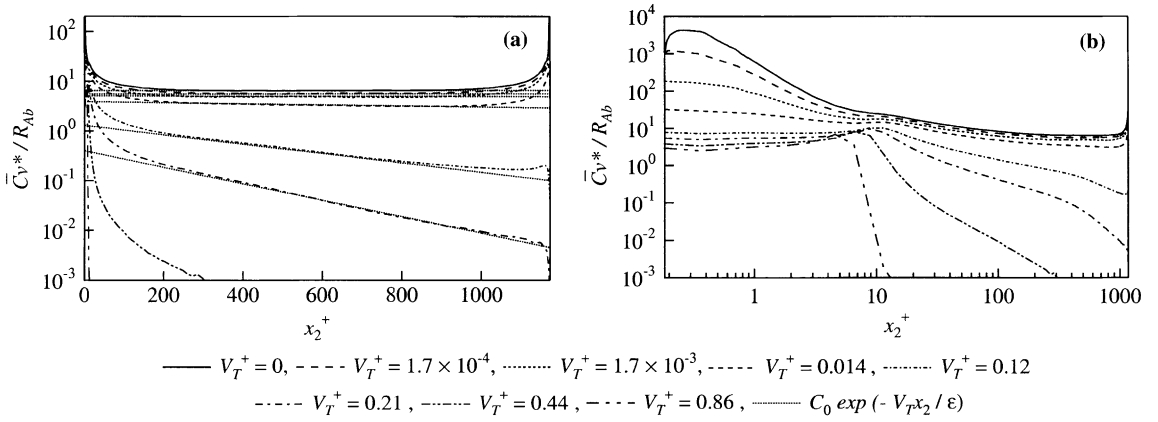

Fig. 10. Concentration profiles for $\tau_p^+ = 20$ plotted against (a) arithmetic and (b) logarithmic abscissae.

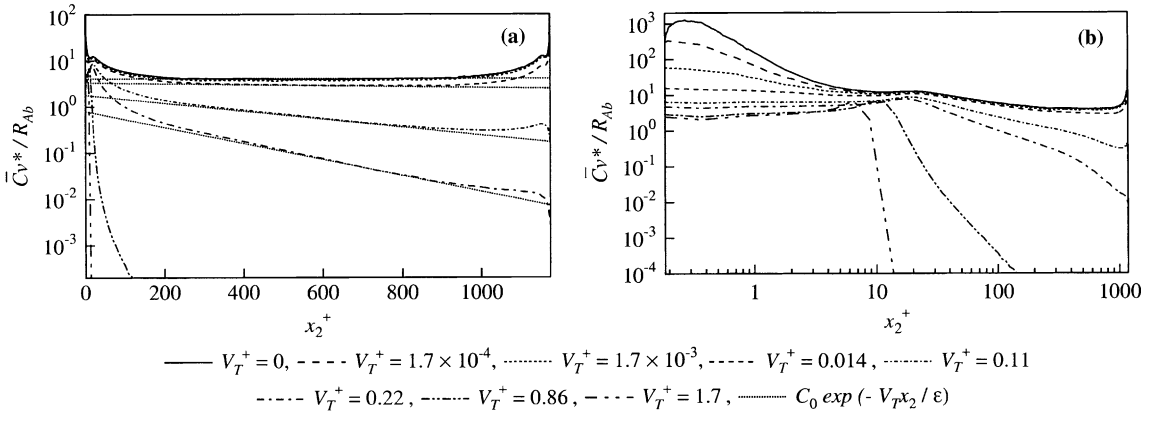

Fig. 11. Concentration profiles for $\tau_p^+ = 40$ plotted against (a) arithmetic and (b) logarithmic abscissae.

This contrasts with the large decreases of the bulk concentration and of the concentration in the center region that are observed for $V_T^+ < 0.01$ with $\tau_p^+ = 5$ and with $\tau_p^+ = 3$. The results for $\tau_p^+ = 10$ show an intermediate behavior.

4.5. Stratification

A concentration field in the saltation regime ($g^+ > 0.04$) represents a stratified configuration, for which the concentration is zero except for the region near the bottom wall. A distinct interface is generated by the same mechanism that generates the secondary maxima, described in Section 3.4. Since fluid turbulence is not affecting particle motion in this regime, the assumption of $\boldsymbol{U} = 0$, used in plotting Fig. 2a and b, can be used to calculate the values of x_2^+ at the interfaces at $\tau_p^+ = 3$ and 20. This calculation is approximate since the fully-developed concentration field in this regime is calculated as the sum of the contributions both from the particles affected by the injection process, described in Fig. 2, and the depositing particles.

4.6. Secondary maxima

Secondary maxima caused by slowdowns of injected particles are observed in the concentration profiles when the dimensionless concentrations at the local maxima are not too large, say $\overline{C}v^*/R_{Ab} < 100$. The distances from the bottom wall to the secondary maxima are $x_2^+ \approx 1.8$ for $0.011 \leqslant V_T^+ \leqslant 0.058$ and $\tau_p^+ = 3$. It is noted that the value of x_2^+ at $\tau_p^+ = 3$ is much smaller than the maximum values of x_2^+ in Fig. 2a. This shows that turbulent mixing acts very rapidly on the injected particles before they reach the distances shown in Fig. 2a (even though the magnitude of the fluid turbulence is very small).

Secondary maxima for $\tau_p^+ = 20$ are found at $x_2^+ \approx 11.5$ for $1.7 \times 10^{-3} \leqslant V_T^+ \leqslant 0.12$. The location decreases with increasing V_T^+ for $V_T^+ > 0.12$. This decrease is not observed for $\tau_p^+ = 3$ because the particle field is in the saltation regime for $V_T^+ > 0.058$. A secondary maximum for $V_T^+ = 0.12$ and $\tau_p^+ = 20$ is seen at $x_2^+ \approx 10$. It is noted that the calculations presented in Fig. 3 indicate that the velocities of particles injected in a quiescent medium are approximately equal to the wall-normal fluid turbulence intensity near the location of the secondary maximum.

4.7. Wall concentration

We have noted that the shape of the concentration profiles can be similar. Thus, the magnitude of the concentration at a given x_2^+ is strongly dependent on the concentration at the wall.

The concentration at $x_2^+ = d_p^+/2$, designated as $\overline{C}_w$, has contributions from both the injected particles, $\overline{C}_{w+}$, and the depositing particles, $\overline{C}_{w-}$:

$$\frac{\overline{C}_w v^*}{R_{Ab}} = \frac{\overline{C}_{w+} v^*}{R_{Ab}} + \frac{\overline{C}_{w-} v^*}{R_{Ab}}. \tag{25}$$

Since the rates of injection are equal to rates of deposition, $R_{Ab} = \overline{C}_{w+} V_2^0 = -\overline{C}_{w-} \overline{V}_d$, and

$$\frac{\overline{C}_w v^*}{R_{Ab}} = \frac{1}{V_2^{0+}} - \frac{1}{\overline{V}_d^+}. \tag{26}$$

When $-\overline{V}_d^+ \ll V_2^{0+}$, $\overline{C}_w v^*/R_{Ab} \cong -1/\overline{V}_d^+$. Fig. 12 presents concentrations at $x_2^+ = d_p^+/2$ for $1.7 \times 10^{-5} \leqslant V_T^+ \leqslant 3.2$ for $\tau_p^+ = 3, 5, 10, 20, 40$. Large changes of $\overline{C}_w v^*/R_{Ab}$ with increasing V_T^+

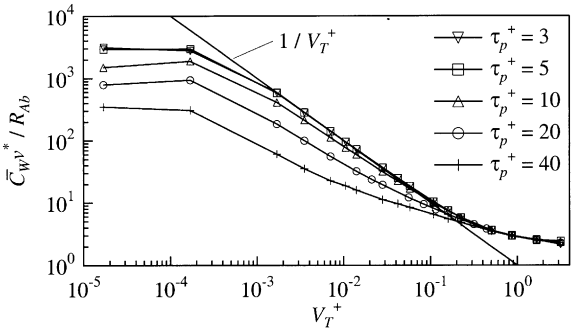

Fig. 12. Concentration at $x_2^+ = d_p^+/2$.

are noted. The values at $V_T^+ = 0$ are, respectively, 3270, 2780, 1180, 628, 284 for $\tau_p^+ = 3$, 5, 10, 20, 40.

For large enough V_T^+ gravitational settling is the dominant mechanism for deposition. The straight line shown in Fig. 12, which represents $1/V_T^+$, gives a good approximation for the wall concentration when $-\overline{V}_d^+ \cong V_T^+$ and $-\overline{V}_d^+ \ll V_2^{0+}$, as indicated by Eqs. (25) and (26). The wall concentrations for $\tau_p^+ = 3$ and 5 are almost the same for all V_T^+. The wall concentrations for $\tau_p^+ = 3$ and 5 equal $1/V_T^+$ for $1 \times 10^{-3} < V_T^+ < 0.2$. The wall concentrations for $\tau_p^+ = 10$ are given by $1/V_T^+$ for $0.1 < V_T^+ < 0.2$.

The concentration at the bottom wall is seen to converge to a maximum value with decreases of τ_p^+ and V_T^+. The dimensionless wall concentrations for $\tau_p^+ = 3$ and 5 are seen to reach this limit for $V_T^+ \leqslant 1.7 \times 10^{-4}$. The maxima for $V_T^+ \to 0$ are consistent with the observation that deposition is controlled by the turbulent motions of the particles and not gravitational settling. The decrease in the dimensionless concentration with increasing τ_p^+ is associated with increased importance of deposition by free-flight. For situations in which a saltation mechanism is dominant ($g^+ > 0.04$) the particles are not in the field long enough to reach free-fall (Mito and Hanratty, 2004a). Thus the dimensionless concentration can exceed $1/V_T^+$ at large V_T^+.

Plots of the ratio of the concentrations at the top and bottom walls are presented in Fig. 13. An interesting aspect of these results is that $\overline{C}_{wt}/\overline{C}_w$ can be much less than unity for situations in which the concentration profiles presented in Figs. 8–11 a appear to be symmetric ($V_T^+ < 10^{-2}$). This is particularly evident for $\tau_p^+ = 3$, 5 at $V_T^+ = 1.7 \times 10^{-4}$. The ratio for $\tau_p^+ = 3$ is not given since, except for extremely small V_T^+, the concentration at the top wall equals zero.

The above observation can be explained by considering that deposition occurs at the bottom wall by turbulent impaction (dominant only for $\tau_p^+ = 3$, 5), by free-flight (dominant for $\tau_p^+ = 20$, 40) and by gravitational settling. At the top wall, gravitational settling inhibits deposition. At $\tau_p^+ = 3$, it prevents deposition when V_T^+ is larger than the turbulent impaction velocities. Thus, deposition by turbulence impaction is unimportant at the top wall for $V_T^+ > 1.7 \times 10^{-4}$, so the only mechanism available is free-flight.

Plots of $\overline{C}_{wt} v^*/R_{At}$, where R_{At} is the rate of atomization at the top wall, are presented in Fig. 14. These dimensionless concentrations equal the reciprocal of the mean velocity of depositing particles. By comparing Figs. 12 and 14 it is noted that the average deposition velocity at the top wall is

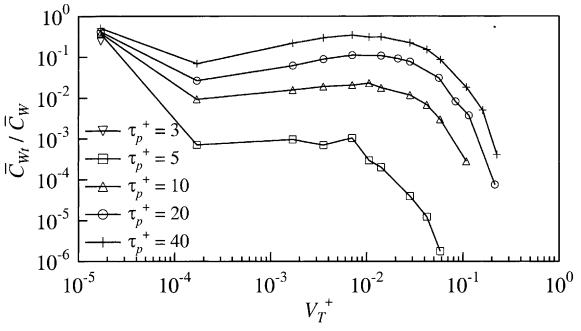

Fig. 13. Ratios of the concentrations at the top and bottom walls.

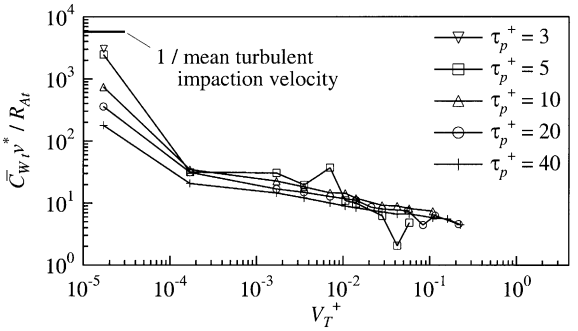

Fig. 14. Concentration at $x_2^+ = 2H^+ - d_p^+/2$.

larger than the average deposition velocity at the bottom wall. This is not understood, but it suggests that larger free-flight velocities are needed to reach the top wall.

4.8. Mass flux balance

Contributions of mechanisms of particle transport in a concentration field can be discussed by using an ensemble-averaged mass balance equation. For a fully-developed field it is given by Eqs. (14) and (16):

$$\overline{C}(V_{tp} + V_g) - \varepsilon \frac{\partial \overline{C}}{\partial x_2} + \text{residual} = 0, \tag{27}$$

where $V_{tp} = -\overline{\tau_p(dV_2/dt)}$ determined from calculations such as shown in Fig. 6, $V_g = -\overline{\tau}_p g$ and a residual term is introduced to include turbulent mixing that cannot be captured by a Boussinesq approximation. Fig. 15a presents dimensionless mass fluxes, $\overline{C}V_{tp}/R_{Ab}$, $\overline{C}V_g/R_{Ab}$ and $-(\varepsilon/R_{Ab})(\partial\overline{C}/\partial x_2)$, in the bottom half of the channel for $\tau_p^+ = 20$ and $V_T^+ = 1.7 \times 10^{-4}$. The turbulent diffusivity for fluid particles is used to calculate the turbulent diffusion flux. In the center region of the channel, $x_2^+ > 350$, turbophoresis is positive and dominant (but it is very small). A mechanism which carries particles in the negative x_2 direction, in order to balance the turbophoresis, is missing. In the region of $x_2^+ < 350$, turbulent diffusion and turbophoresis are the main mechanisms. Turbulent diffusion carries particles in the positive x_2 direction. The negative turbophoresis observed at $x_2^+ < 80$ causes a buildup of particles in the near-wall region. Gravitational transport becomes important only in the vicinity of the bottom wall ($x_2^+ < 0.3$), at which it is balanced with turbophoresis. The same features are observed throughout the region where the concentration profiles are symmetric ($V_T^+ < 0.01$).

Fig. 15b presents dimensionless mass fluxes in the bottom half of the channel for $\tau_p^+ = 20$ and $V_T^+ = 0.014$, for which asymmetry starts appearing in the concentration field. Increases of gravitational transport at all x_2^+ are noted. All of the three fluxes are important in the region $x_2^+ > 350$. Turbulent diffusion transports particles in the positive x_2 direction. Negative turbophoresis observed for $x_2^+ < 80$ carries particles into the near-wall region. Small negative values of turbulent diffusion, observed at $x_2^+ \approx 10$, are caused by the secondary maximum.

The contribution of gravitational transport increases with increasing V_T^+ as seen by comparing Fig. 15b with Fig. 15c. Gravitational transport is mainly balanced with turbulent diffusion for

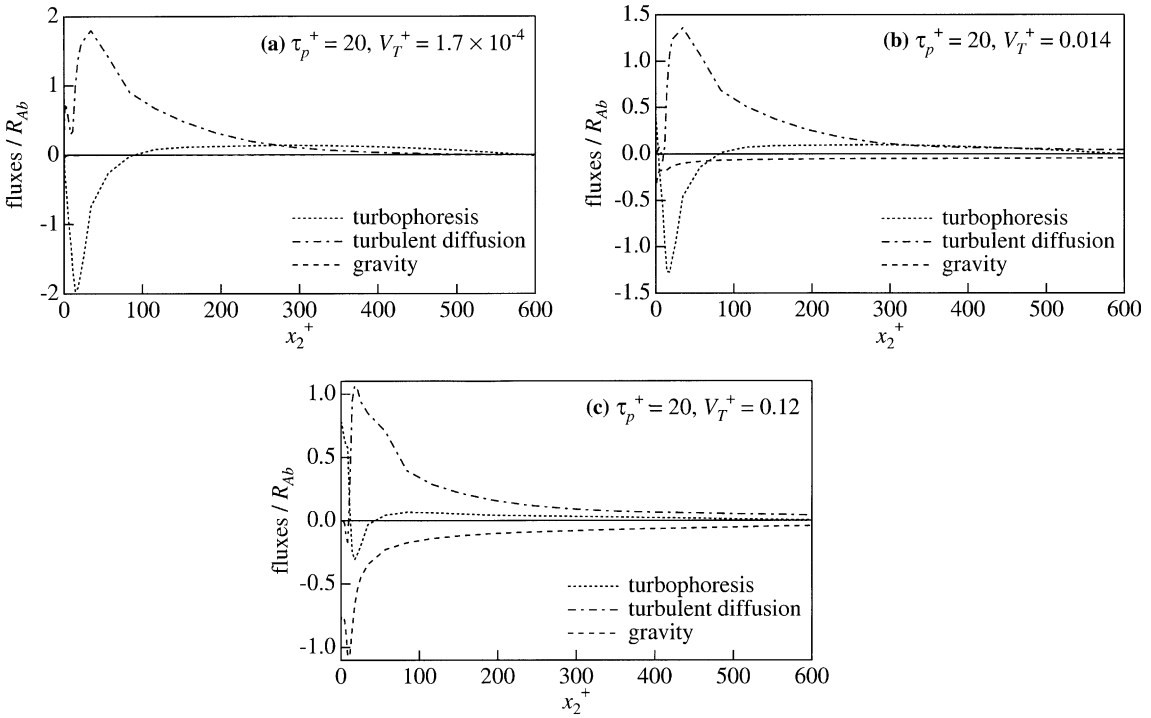

Fig. 15. Dimensionless mass fluxes for $\tau_p^+ = 20$. (a) $V_T^+ = 1.7 \times 10^{-4}$, (b) $V_T^+ = 0.014$ and (c) $V_T^+ = 0.12$.

$\tau_p^+ = 20$ and $V_T^+ = 0.12$ except for the vicinity of the bottom wall, where gravity and turbophoresis are the important transport mechanisms. Negative turbophoresis, observed for $x_2^+ < 80$, still contributes to a transport of particles into the near-wall region.

Fig. 16 presents residuals in the mass flux balances, made dimensionless with R_{Ab}, for the cases that have been discussed above. It is noted that the curves show similar shapes and that the residual decreases with increasing V_T^+. The shapes of the residual curves also do not change with changes in τ_p^+. This suggests that the mass flux residual could be deterministically given. It is noted that the residual for $V_T^+ = 0.12$ is almost zero for large x_2^+. In the region of $x_2^+ < 20$ positive

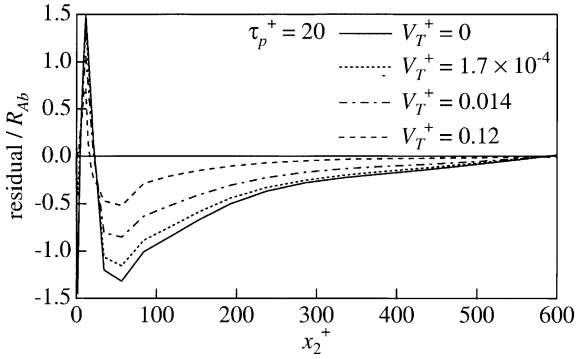

Fig. 16. Dimensionless residuals in the mass flux balances for $\tau_p^+ = 20$.

residual fluxes are observed. A small region with negative residuals is seen in the vicinity of the bottom wall for $V_T^+ = 1.7 \times 10^{-4}$.

5. Discussion

5.1. Effect of gravity on the concentration field

The fully-developed concentration field associated with the horizontal flow of a dilute suspension of spherical particles has been analyzed in order to obtain a better understanding of deposition and mixing. The principal contribution of this paper is that it presents concentration profiles for a wider range of V_T^+ than had previously been addressed. An analogue of a fully-developed gas–liquid annular flow is considered for which the rate of injection of particles from the wall equals the rate of deposition. Gravity causes the rate of deposition to be much smaller at the top wall than at the bottom wall and an asymmetric distribution of the particles can result. This influence is characterized by a dimensionless gravity, g^+, or by a dimensionless settling velocity, V_T^+. Gravitational settling was found to have a small effect on the particle turbulence for the range of $g^+ = 0$–0.04 for which saltation is not a dominant mechanism for particle mixing.

Gravity influences the concentration profiles and the deposition constant by increasing the average velocity with which particles deposit at the bottom wall and by causing asymmetries in the profile.

As shown in Eq. (26), the dimensionless concentration at the bottom wall, $\overline{C}_w v^*/R_{Ab}$, decreases with the increasing magnitude of the deposition velocity, $-\overline{V}_d$. The deposition velocity has a minimum value of $-\overline{V}_d = 1.7 \times 10^{-4}$, which is governed by the fluid turbulent velocity fluctuations at $x_2^+ = d_p^+/2$. This dictates the maximum value of the dimensionless wall concentration. The wall concentration and the deposition velocity for $\tau_p^+ = 3$, 5 are unchanged for cases in which $-\overline{V}_d < 1.7 \times 10^{-4}$. For larger τ_p^+ the deposition velocity increases because of contributions by free-flight, so the dimensionless concentration at the wall decreases.

Particles tend to accumulate close to the wall because of turbophoretic transport. The concentration can have a maximum at a short distance from the wall where turbophoresis can be very small, so that a thin boundary layer can exist for which particles are transported to the wall by turbulent diffusion.

This boundary layer disappears when $V_T^+ > 1.7 \times 10^{-4}$, that is when the settling velocity is larger than the turbulent impaction velocity. The deposition velocity increases and the concentration at the wall decreases with increasing V_T^+. Noticeable asymmetries in the concentration profiles are observed for $V_T^+ > 0.01$. The degree of asymmetry increases with increasing V_T^+. A region in the center of the channel exists in which the $\ln \overline{C}$ varies linearly with x_2^+. This can be interpreted as resulting from a balance between gravitational settling and turbulent diffusion, represented by the product of a turbulent diffusivity, ε, and the concentration gradient, $\partial\overline{C}/\partial x_2$. In this comparison ε is assumed to be proportional to the product of the height of the channel and the friction velocity, and equal to the fluid diffusivity. This interpretation is, somewhat, flawed because it ignores the turbophoretic flux, which can be significant.

Deposition at the top wall is impeded by gravity so that, except for $V_T^+ = 0$, deposition occurs only by free-flight particles with high velocities. As a consequence the rate of deposition and the

concentration at the top wall are much smaller than what is observed at the bottom wall. Turbophoresis causes a buildup of particles close to the top wall. Thus, if V_T^+ is not too large the profiles give the appearance of being symmetric even though the deposition rates at the top and bottom walls are different.

The dimensionless concentration of injected particles at the wall is defined as $\overline{C}_{w+}v^*/R_{Ab} = 1/V_2^{0+} = 1$. As these injected particles move away from the wall, their concentration increases because they slow down. Eventually they get mixed by fluid turbulence. This can result in the creation of a secondary maximum. For the situations considered in this paper, this maximum occurs close to the wall.

5.2. Use of a diffusion model

As shown in Section 3.2 the turbophoretic and gravitational fluxes for the fully-developed flow considered in this paper are balanced by a flux due to turbulent mixing, $\overline{v_2 c}$. This paper explored the possibility of representing the turbulent mixing by assuming

$$\overline{v_2 c} = -\varepsilon \frac{\partial \overline{C}}{\partial x_2}, \tag{28}$$

where the turbulent diffusivity, ε, is assumed to be equal to that of the fluid. It is found that a balance cannot be obtained.

One possibility for this discrepancy is that the turbulent diffusivity needs to be modified. Fig. 17a presents calculated ε needed to obtain a balance. As already shown by Mito and Hanratty (2004b)

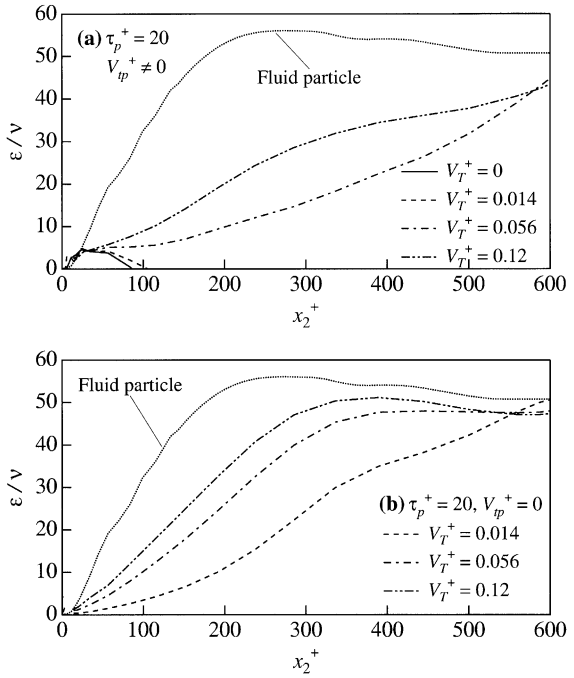

Fig. 17. Turbulent diffusivities for $\tau_p^+ = 20$ calculated with the assumptions of (a) $V_{tp} \neq 0$ and (b) $V_{tp} = 0$.

calculations for $V_T^+ = 0$ yield the unphysical result of negative values of ε for $x_2^+ >$ ca. 80. Similar results are obtained for $V_T^+ = 0.014$. For $V_T^+ = 0.056$ and 0.12 the needed values of ε are much smaller than those for the fluid. The strong effect of V_T^+ on ε is not consistent with its observed small effect on the particle turbulence, shown in Fig. 5. Fig. 17b presents calculations of ε/ν for $\tau_p^+ = 20$ if turbophoretic effects are ignored. The ε/ν for $V_T^+ = 0.056$ and 0.12 are close to values for the fluid diffusivity in the central regions of the channel, which is consistent with the success of Eq. (17) in representing concentration variations in the outer part of the flow. However, a large effect of V_T^+ on ε/ν is still observed and the justification for neglecting turbophoretic effects is not clear, especially since they are needed to explain the accumulation of particles close to the wall.

The failure of a Boussinesq approximation to represent turbulent mixing should not be surprising. The inability of an eddy viscosity model to represent the Reynolds stress has been noted in several instances. This has led to the development of Reynolds stress closure models. This unsuccessful modeling of $\overline{v_2 c}$ probably reflects the observation that the particle turbulence may not be in equilibrium with the fluid turbulence, because of the inertia of the particles, and that large scale mixing motions, such as free-flights, are not captured by a Boussinesq approximation.

One way of representing the mixing (Mito and Hanratty, 2004b) is to modify Eq. (13) to include sources and sinks

$$\frac{\partial}{\partial x_2}\left[\overline{C}(V_{tp} + V_g) - \varepsilon\frac{\partial \overline{C}}{\partial x_2}\right] = S. \tag{29}$$

Here, a negative S indicates a sink which might be pictured as a disengagement of the particle from the fluid turbulence, such as would occur at the start of a free-flight. A positive S might indicate an end of a free-flight where the particle motion becomes closely related to the fluid turbulence.

Fig. 18 shows calculated values of dimensionless sources, $Sv/R_{Ab}v^*$, calculated from Eq. (29) for $\tau_p^+ = 20$ by using the fluid diffusivity to represent ε. Values of $V_T^+ = 0$, 1.7×10^{-4}, 0.014 and 0.12 are explored. Four regions can be identified. Region I, $55 < x_2^+ < 590$, is a very weak net sink. Region II, $11 < x_2^+ < 55$, which contains net sources, extends roughly from the outer edge of the viscous wall layer to just outside the viscous sublayer. Region III, which contains net sinks, extends from $x_2^+ \cong 1.5$ to $x_2^+ \cong 11$. Similar regions with approximately the same boundaries have been observed for other τ_p^+. The interpretation of these results and, in particular, the explanation of the similarity is not clear-cut. Region III may represent locations where particles, on average, start free-flights which end in the viscous sub-layer or at the wall. Region II could represent the end point of weak large-scale motions that bring particles from the outer flow to the wall region and the location where particles injected from the wall become entrained in the turbulence. Region IV, which contains net sources, may account for the accumulation of the particles that have been in free-flights. The magnitude of the sources increases with decreasing V_T^+. This could reflect the fact that the accumulation of particles in the near-wall region increases with decreasing V_T^+.

5.3. Final remarks

The modeling of turbulent mixing emerges as a critical issue in interpreting concentration profiles. The resolution could lie in the development of a differential equation for $\overline{v_2 c}$ or in a judicious use of two-fluid equations. However, it is also possible that the soundest theoretical approach to

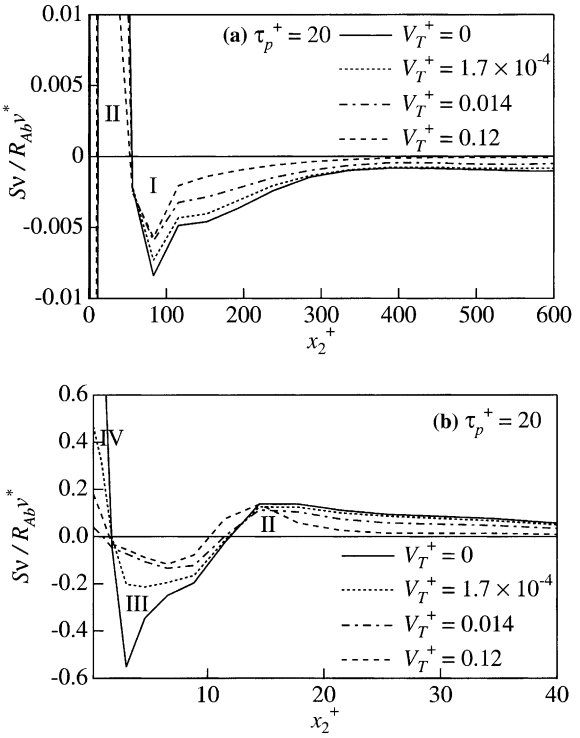

Fig. 18. Sources and sinks for $\tau_p^+ = 20$ (a) in the half-height of the channel and (b) in the near-wall region.

describing these dilute suspensions is the use of Lagrangian methods which model the fluid turbulence seen by the particles.

Acknowledgments

This work is supported by DOE under grant DEFG02-86ER 13556. Computer resources have been provided by the National Center for Supercomputing Applications located at the University of Illinois.

References

Caporaloni, M., Tampieri, R., Trombetti, R., Vittori, O., 1975. Transfer of particles in nonisotropic air turbulence. J. Atmos. Sci. 32, 565–568.

Cerbelli, S., Giusti, A., Soldati, A., 2001. ADE approach to predicting dispersion of heavy particles in wall-bounded turbulence. Int. J. Multiphase Flow 27, 1861–1879.

Graham, D.I., 1996. On the inertia effect in eddy interaction models. Int. J. Multiphase Flow 22, 177–184.

Iliopoulos, I., Mito, Y., Hanratty, T.J., 2003. A stochastic model for solid particle dispersion in a nonhomogeneous turbulent field. Int. J. Multiphase Flow 29, 375–394.

Lun, C.K.K., Liu, H.S., 1997. Numerical simulation of dilute turbulent gas-solid flows in horizontal channels. Int. J. Multiphase Flow 23, 575–605.

McCoy, D.D., Hanratty, T.J., 1977. Rate of deposition of droplets in annular two-phase flow. Int. J. Multiphase Flow 3, 319–331.

Mito, Y., Hanratty, T.J., 2002. Use of a modified Langevin equation to describe turbulent dispersion of fluid particles in a channel flow. Flow Turbul. Combust. 68, 1–26.

Mito, Y., Hanratty, T.J., 2003a. Lagrangian stochastic simulation of turbulent dispersion of heat markers in a channel flow. Int. J. Heat Mass Trans. 46, 1063–1073.

Mito, Y., Hanratty, T.J., 2003b. A stochastic description of wall sources in a turbulent field: Part 1. Verification. Int. J. Multiphase Flow 29, 1373–1394.

Mito, Y., Hanratty, T.J., 2004a. A stochastic description of wall sources in a turbulent field: Part 2. Calculation for a simplified model of horizontal annular flows. Int. J. Multiphase Flow 30, 803–825.

Mito, Y., Hanratty, T.J., 2004b. Concentration profiles in a turbulent suspension when gravity is not affecting deposition. Int. J. Multiphase Flow 30, 1311–1336.

Moser, R.D., Kim, J., Mansour, N.N., 1999. Direct numerical simulation of turbulent channel flow up to $Re_\tau = 590$. Phys. Fluids 11, 943–945.

Oesterle, B., Petitjean, A., 1993. Simulation of particle-to-particle interactions in gas-solid flows. Int. J. Multiphase Flow 19, 199–211.

Paras, S.V., Karaberas, A.J., 1991. Droplet entrainment and deposition in horizontal annular flow. Int. J. Multiphase Flow 17, 455–468.

Reeks, M.W., 1983. The transport of discrete particles in inhomogeneous turbulence. J. Aerosol Sci. 14, 729–739.

Sommerfeld, M., Zivkovic, G., 1992. Recent advances in the numerical simulation of pneumatic conveying through pipe systems. In: Hirsch, Ch., Periaux, J., Onate, E. (Eds.), Computational Methods in Applied Sciences. In: Invited Lectures and Special Technological Sessions of the First European Computational Fluid Dynamics Conference and the First European Conference on Numerical Methods in Engineering, Brussels, pp. 201–212.

Sommerfeld, M., Kohnen, G., Rüger, M., 1993. Some open questions and inconsistencies of Lagrangian particle dispersion models. Proceedings of the Ninth Symposium on Turbulent Shear Flows, Kyoto Japan, Paper No. 15–1.

Sommerfeld, M., 2003. Analysis of collision effects for turbulent gas-particle flow in a horizontal channel: Part I. Particle transport. Int. J. Multiphase Flow 29, 675–699.

Williams, L.R., Dykhno, L.A., Hanratty, T.J., 1996. Droplet flux distributions and entrainment in horizontal gas–liquid flows. Int. J. Multiphase Flow 22, 1–18.

Young, J.B., Hanratty, T.J., 1991. Optical studies on the turbulent motion of solid particles in a pipe flow. J. Fluid Mech. 231, 665–688.

Young, J., Leeming, A., 1997. A theory of particle deposition in turbulent pipe flow. J. Fluid Mech. 340, 129–159.

Zhang, H., Ahmadi, G., 2000. Aerosol particle transport and deposition in vertical and horizontal turbulent duct flows. J. Fluid Mech. 406, 55–80.